Oil Shale, 2010, Vol. 27, No. 2, pp. 164–178
doi: 10.3176/oil.2010.2.06
ISSN 0208-189X

AN EXPERIMENTAL STUDY ON DEVOLATILIZATION OF OIL SHALE PARTICLES UNDER FLUIDIZED-BED OXIDIZING CONDITIONS

WANG QING*, WANG XIAOLEI, SUN BAIZHONG,
QIN HONG, LIU HONGPENG, LI SHAOHUA

Northeast Dianli University
Jilin 132012, China

The devolatilization characteristics of Wangqing oil shale were studied in a laboratory-scale fluidized-bed unit at 600–904 °C. The characteristics of furnace temperature variation, preheating time and burnout of particles were studied in detail after oil shale being injected. The effect of batch mass, bed temperature, fluidization velocity, and moisture content on volatile combustion was also investigated. The experimental results show that the combustion of volatiles was mostly influenced by the bed temperature and reaction mechanism. The combustion time was in accordance with empirical model. A new modified model for combustion time of volatiles related to temperature, particle size, and reaction mechanisms was proposed. The results calculated with this model are in agreement with experimental data, and it can be used to predict combustion time of volatiles for the high-temperature region.

Introduction

Oil shale, categorized as a solid fossil fuel, is a complex heterogeneous mixture of a wide range of minerals [1]. The combustion mechanism of oil shale is complex due to its composition. Most of the previous works on solid fuels were focused on combustion of carbon, char, coke, devolatilized coal and coal particles [2, 3]. Until recently, there is some lack of knowledge about the devolatilization mechanism of oil shale in fluidized bed.

When oil shale particles are introduced into a hot fluidized bed of solid particles, the following steps in quick succession have been observed [3, 4]:

1. The particles mix with bed particles and hot flowing gas stream.
2. The particles heat up to some temperature lower than the bed temperature. Depending upon the reaction conditions and shale type, the preheating period takes a few seconds.
3. Evolution of water and volatile materials during the preheating period.

* Corresponding author: e-mail *rlx888@126.com*

4. A luminous flame surrounds the particles. The particles appear to be supported by the surrounding flame. The brightness degree of shale particles depends on reaction conditions and content of volatiles.
5. Ignition and combustion of the residual organic solid material (char) associated with fragmentation of particles take place. In general, the brightness increases with increasing excess air and fluidizing velocity.

When considering the devolatilization in fluidized bed, three resistances in series can be identified: the interphase resistance to oxygen transfer from the bubble phase to the particulate phase; the resistance to oxygen diffusion from the particulate phase to the surface of the particle; the resistance to the combustion reaction at the surface of the particle [4].

Therefore, the devolatilization of oil shale includes the phase of preheating, the phase of volatiles' combustion and the phase of burnout. The devolatilization may be controlled by three main factors: heat transfer to and within the particle, chemical kinetics of pyrolysis, and mass transfer of volatile products within the particle [5].

Ragland and Weiss [6] studied the burnout behavior of single coal particles suspended in the air at elevated temperatures. Devolatilization time was measured as the time between ignition and extinction of the volatiles' flame. A similar method for measuring devolatilization time was employed by Pillai [4] when investigating the evolution and combustion of volatiles and char in a fluidized bed using large coal particles. Khraisha et al. [3] investigated the characteristics of burnout of oil shale in fluidized bed. Bai et al. [7] investigated burnout characteristics of oil shale blended with semi-coke. The experimental devolatilization time or burnout time in these investigations was correlated by:

$$t = ad^b \tag{1}$$

This is an empirical model, where t is combustion time or burnout time of volatiles, a and b are constants, d is particle diameter. Many different values of b were obtained with many measuring instruments and measuring methods by many researchers [8]. $b = 1.5$ was obtained by Ragland and Weiss [6], $b = 0.3–1.8$ by Pillai [4], $b = 0.5–1.51$ by Khraisha [3] and $b = 0.5–1.25$ by Bai [7]. Assuming that core shrinking is controlled by kinetics, $b = 1$. If internal heat transfer controls devolatilization, the value of b should be 2; on the other hand, if external heat transfer governs devolatilization, b will lie between 1 and 2, depending on the size of the particle [8]. If there is internal mass transfer control, the resulting value of b is also 2. This model is rough, since the effects of pyrolysis chemistry and transport processes are not treated separately, but they are included in the constants. Therefore, the above model is helpful in studying the devolatilization of oil shale under oxidizing condition [9, 10].

It has been pointed out that the visual observation is more accurate than the method of analyzing volatiles' yield with instruments [4]. This is because combustion processes are complex in nature and product yield, which could

disturb instruments during reactions. For example, carbon monoxide and carbon dioxide may diffuse away from the particle during the period of reaction.

The purpose of this paper was to study devolatilization characteristics of oil shale from Wangqing under fluidized-bed oxidizing conditions. In this study, we investigated the preheating of particles, combustion of volatiles, and burnout of particles under different experimental conditions. This paper presents a new modified model for calculating combustion time of volatiles that processes the data efficiently.

Experimental

Experimental facility

A laboratory-scale fluidized bed as shown in Fig. 1 was used in this research. The main unit of the setup is the fluidized-bed combustor, which is a stainless-steel tube of 51 mm in internal diameter and surrounded by a thick heat insulator. The reactor was connected with a tube of the same internal diameter to preheat the incoming gas. The fluidized bed was equipped with a gas distributor made of a stainless-steel wire mesh fixed at the bottom of the bed. The fluidized bed was mounted vertically and the gas pre-heater was mounted horizontally within an electrically heated furnace. Air was introduced into the base of the gas pre-heater *via* a rotameter. A thermocouple fixed 55.5 mm above gas distributor was used to record temperature within the fluidized bed and to send the signal of temperature to the data collection

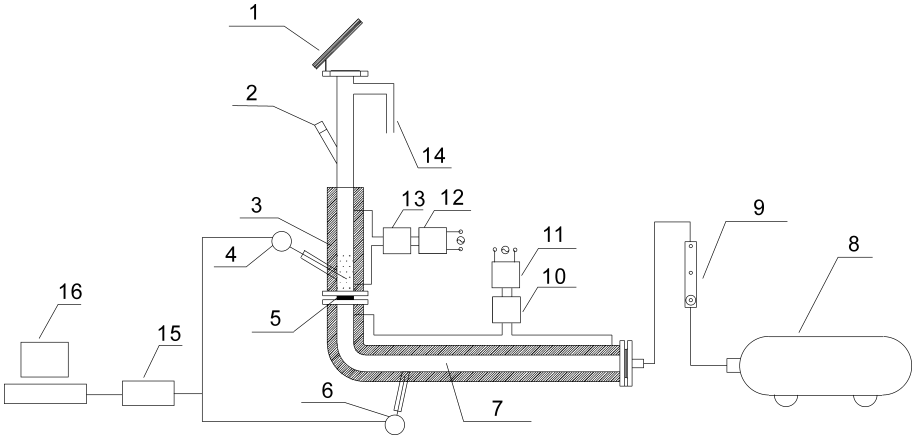

Fig. 1. Bench-scale fluidized-bed reactor.

1 – mirror; 2 – feeder; 3 – heat insulator; 4 – thermocouple; 5 – gas distributor; 6 – thermocouple; 7 – preheating section; 8 – air compressor; 9 – rotameter; 10 – temperature controller; 11 – voltage controller; 12 – voltage controller; 13 – temperature controller; 14 – discharge gate; 15 – data collection system; 16 – computer.

system. The heating section and preheating section temperature were controlled by the temperature controller separately to get the accurate temperature. A mirror was fixed above the reactor tube to observe the behavior of shale particles after injection.

Sample preparation

Oil shale from Wangqing was used for this research. Chemical analyzes of sample are as follows (mass%):

proximate analysis: M_{ad} – 1.26, V_{ad} – 16.52, A_{ad} – 81.12, FC_{ad} – 1.1, $Q_{ar,net}$ – 3528.9 J/g;

ultimate analysis: C_{ad} – 9.68, H_{ad} – 0.75, N_{ad} – 0.13, S_{ad} – 0.29 (ad – air dry basis).

A jaw crusher was used to crush the samples, which were sieved to obtain the required particle size (0.25–0.315 mm, 0.315–0.355 mm, 0.355–0.5 mm, 0.5–0.63 mm, 0.63–0.8mm , 0.8–1mm , 1–2.18 mm, 2.18–2.8 mm, 2.8–4.8 mm, 4.8–5.9 mm) with a set of Taylor series sieves. The bed material was quartz sand (120 g) sieved to the size range of 0.45–0.71 mm.

Experimental process

The operating conditions in this research are shown in Table 1. The bed temperature was controlled by adjusting the electrical power. When the bed temperature attained to target temperature and steady state, a weighed charge of shale particles was dropped into the hot bed and a stopwatch was started simultaneously to record the time of flame appearance (t_p), the time of flame extinction (t_p+t_{vc}) and the burnout time (t_b), where t_p represents preheating time of particle (defined as the time between injection of oil shale and appearance of volatiles' flame), t_{vc} represents combustion time of volatiles (defined as the time between appearance and extinction of volatiles' flame), and t_b represents burnout time (defined as the time between appearance of volatiles' flame and disappearance of any luminous residue). The experiment was generally repeated at least twice to reduce errors, and the mean of the closest two results was used. The observed maximum variance in devolatilization time recordings of the three was within 10% of the averaged values, indicating that the experiments are repeatable.

Table 1. **Operating conditions**

Operating condition	Air flow rate, m^3/ h	Moisture content	Batch mass, g	Bed temperature, °C
A	0.7	air dry basis	4	904
B	0.7	air dry basis	4	600–904
C	0.7	air dry basis	2	904
D	1.2	air dry basis	4	904
E	0.7	dry basis	4	904
F	0.7	air dry basis	4	850

Results and discussion

General phenomenon

The following phenomenon was observed in the experimental study. If the fluidization velocity, namely approach of fluidized bed to fixed bed, was low enough, the plume flame surrounding the particles could be observed. When the fluidization velocity was higher, the plume flame was not obvious and the shape of the flame was not regular either because of airflow disturbance. The volatiles released faster with increasing temperature. Much "white smoke" flew faster with increasing fluidization velocity. This suggested that volatiles cannot be burned out in bed but most volatiles would be burned out in the space above the bed. So the furnace for oil shale combustion should have a sufficient height to ensure the heat be absorbed sufficiently to improve combustion efficiency [11].

The fragmentation of shale particles was observed. Figure 2 shows the shape of original sample particle (Fig. 2a) and that after burnout (Fig. 2b). The shale particles tended to produce small fragments slightly only rather than to fragment into much larger individual pieces. Once the gaseous volatile matter within a solid particle is formed, it will cause a higher pressure in the shale particles. Meanwhile, an impulsive force is made by the surrounding particles, and thermal stress is caused by a temperature gradient within the shale particles [12]. The ash content of the sample is high and volatiles' content is low, and this may be the major reason of the insignificant fragmentation.

(a) (b)

Fig. 2. Comparison of particle shape between original sample (a) and after burnout (b) at 904 °C under operating condition A.

Variation characteristic of furnace temperature

Figure 3 presents variation in temperature of bed after oil shale injection at operating condition A. After injection, the bed temperature was slightly decreased for 1–6 °C because of the disturbance of thermal equilibrium in the preheating stage [11]. Then the temperature increased rapidly for 4–13 °C because of the combustion of volatiles and carbon residue. The

variation degree of temperature decreased as particle size decreased. This is mainly because the elutriation of particles, which induce some particles to burn at the top of the furnace, is more obvious with decreasing particle size.

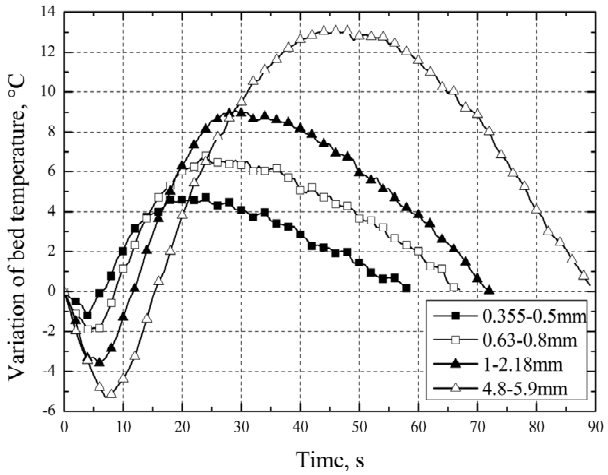

Fig. 3. Variation of bed temperature after injection of particles of different size at 904 °C under operating condition A.

Characteristic of preheating time

Preheating time (t_p) of the sample under operating condition B is shown in Fig. 4. The preheating time decreased as the temperature increased and this variation degree decreased after 800 °C. This is because the effect of high temperature on heating rate is significant and the sample can reach ignition temperature easier.

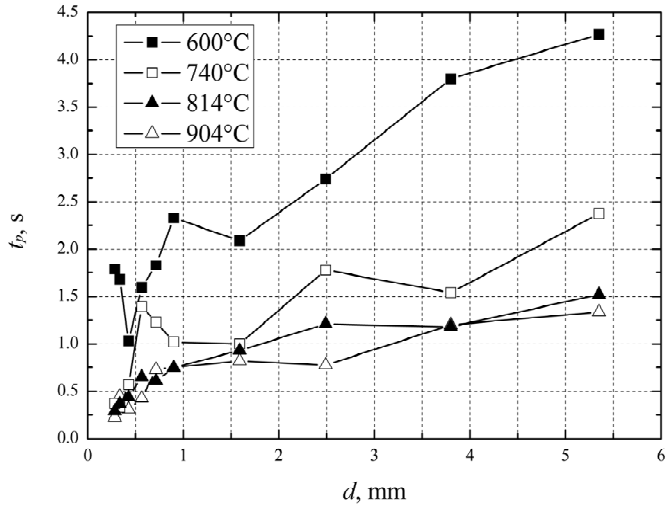

Fig. 4. Preheating time versus particle size of oil shale under operating condition B.

Characteristic of burnout time

The burnout time (t_b) of oil shale was also measured roughly under operating condition B as shown in Fig. 5: a significant tendency for t_b to decrease with increasing temperature for the same particle size. The increasing temperature has a greater effect on t_b as the particle size increases. This is mainly because the combustion of the volatiles can significantly increase the particle temperature during devolatilization and increase volatile yields under oxidative conditions [7].

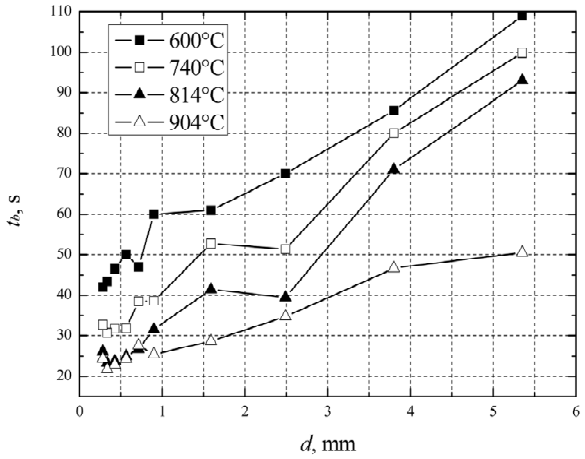

Fig. 5. Burnout time versus particle size of oil shale under operating condition B.

Effect of batch mass on volatile combustion time

Figure 6 shows the results plotted as volatile combustion time against mean particle size (d) of oil shale and their empirical fitting curve under operating

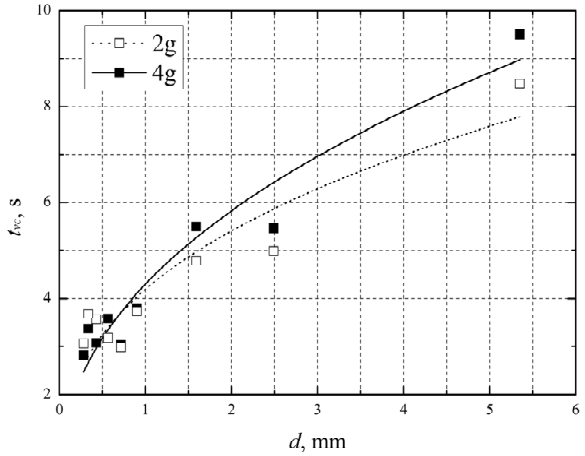

Fig. 6. Volatile combustion time of the batch mass (2 g and 4 g) under operating conditions A and C.

conditions A and C. The batch mass and t_{vc} do not have a simple linear relationship. This is mainly due to the complex reactions. The t_{vc} has a little increase as charge decreases for particle size >1.5 mm, and no significant changes of time were observed for particle size <1.5 mm. It is possible that the devolatilization in the case of small particle size is controlled by intrinsic kinetics. In general, the batch mass has only a weak effect on volatile combustion time.

Effect of moisture content on volatile combustion time

The effect of shale moisture content on t_{vc} (air-dry basis and dry basis) is shown in Fig. 7. The operating conditions are A and E. Because the heating rate in fluidized bed is high, one can assume that the evolution of moisture takes place immediately once the oil shale is fed into the bed [13]. A little change of t_{vc} was observed for smaller particle sizes. Particles with higher moisture content show a slight lower combustion rate of volatiles, especially for smaller particles. Ross [5] has found that when the moisture content increases, its effect on t_{vc} is more pronounced, as would be expected as more water must be evaporated from the particle. Since the moisture content of oil shale is less (M_{ad} = 1.26%), its effects on t_{vc} are not significant under the current condition.

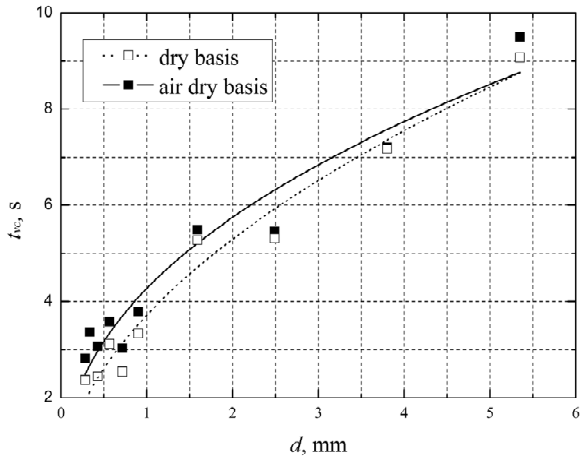

Fig. 7. Volatile combustion time of air-dry and dry particles under operating conditions A and E.

Effect of fluidization velocity on combustion time of volatiles

The effect of fluidization velocity on volatile combustion time and their empirical fitting curve is shown in Fig. 8. The operating conditions are A and D. Fluidization velocities under conditions A and D are 2.38 cm/s and 4.08 cm/s, respectively. An unexpected result is observed that t_{vc} changed little for most particle sizes while the fluidization velocity increases nearly

twice for the same particle size. t_{vc} decreases a little under higher fluidization velocity. At higher fluidization velocities the rate of volatile matter release is slightly higher because of better convective heat transfer to the particle [14]. These results show that fluidization velocity is not the main controlling factor of volatile combustion.

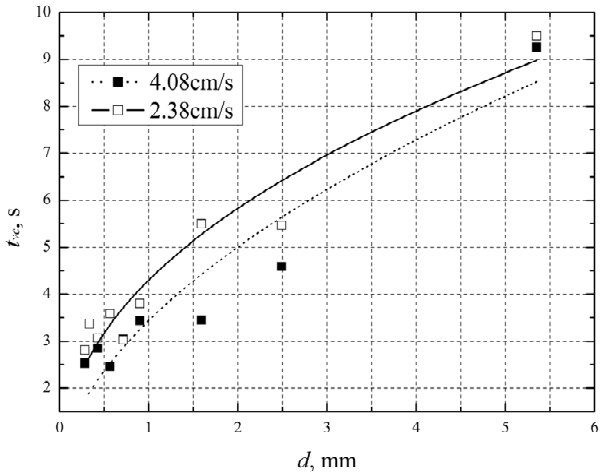

Fig. 8. Comparison of t_{vc} at different fluidization velocity under operating conditions A and D.

Relationship between t_{vc} and d

The relationship between t_{vc} and d and their empirical fitting curve under operating condition B is shown in Fig. 9. As expected, t_{vc} increases as particle size increases at the same temperature. It is due to the fact that as the particle size increases, the specific surface area of the sample of the same quality is less and the contact of the area with oxygen in the process of burning is less. This reduces the rate of combustion and prolongs t_{vc}. Moreover, as ash shell would be produced on the surface of a large particle during combustion making the resistance to oxygen diffusion from the particulate phase to the surface of the particle to increase, t_{vc} increases. t_{vc} decreases as the temperature increases, the particle size being the same. Values of a and b by regression are tabulated for four temperatures in Table 2.

Value of a decreases as the temperature increases. This indicates that a was affected by temperature under certain conditions. This result is consistent with that reported by Saatamoinen [10]. Value of b changes in the range of 0 to 1, which indicates that the reaction rate is not only controlled by a single process but it may be the rate-limiting step in a mixed regime between chemical reaction and heat transfer control. The value of b changes a little after 740 °C, but it changes a lot at 600 °C. Two main factors are important. First, physical absorption plays a significant role at low temperatures while chemical adsorption plays a significant role at high temperature

[15]. Second, the yield of some components will improve with increasing temperature when a lot of secondary reactions occur [16]. So the reaction mechanisms in the high-temperature region and low-temperature region may be different. The value of *b* decreases with increasing temperature in the high-temperature region. This result agrees with the findings by Paul [17].

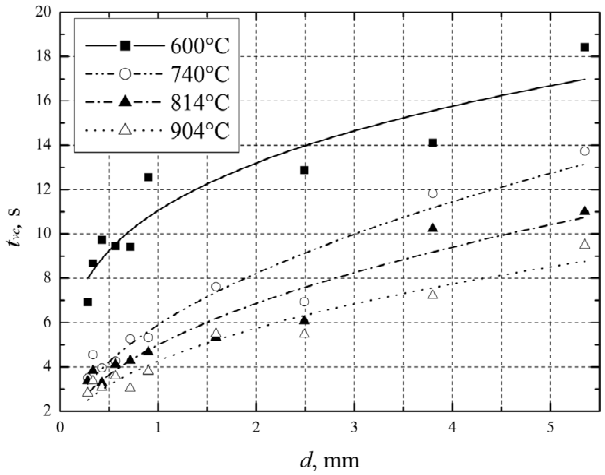

Fig. 9. Relationship between volatile combustion time and particle size under operating condition B.

Table 2. **The value of *a* and *b* by regression at four temperatures**

Temperature, °C	*a*	*b*	R^2
600	11.05	0.26	0.8807
740	5.90	0.48	0.9274
814	5.00	0.46	0.9162
904	4.27	0.43	0.9308

Mathematical model for combustion of volatiles

Establishment of the model

Generally, from Eq. (1), we can give many values of *a* by experiments, where *a* is constant under some operating condition. From that we can estimate the value of *a* for some operating conditions from the average value of *a*. According to this method, we can get the value of *a* from Table 2:

$$a = \overline{a} = \frac{11.05 + 5.90 + 5.00 + 4.27}{4} = 6.56\,. \tag{2}$$

Substituting the value of *a* from Eq. (1) into Eq. (2) gives

$$t_{vc} = \overline{a} d^{\,b}\,, \tag{3}$$

where Eq. (3) is called model I.

The constant *a* in the model I is independent of reaction conditions and does not associate with main controlling factors of reactions. In this research, the value of *a* decreases with increasing temperature *T*. Neglecting other factors and assuming *a* is a function of *T*, namely

$$a = f(T)\,. \tag{4}$$

Plotting *a* versus *T* which are obtained from Table 2 it can be found that *a* and *T* are in agreement with empirical model. The fitting curve is shown in Fig. 10.

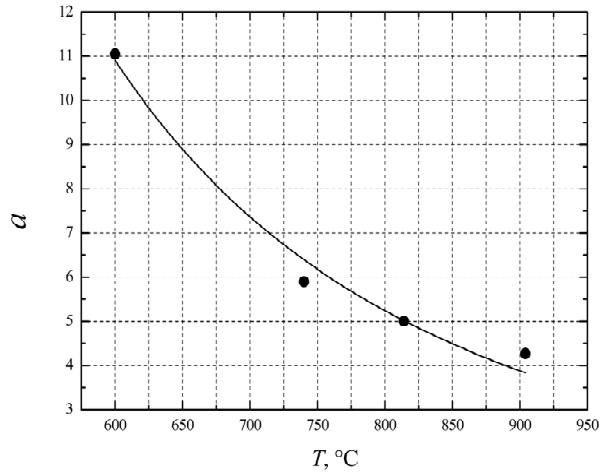

Fig. 10. The fitting curve of *a* and *T*, R^2 = 0.9764.

Assuming

$$a = mT^n\,, \tag{5}$$

evaluating *m* and *n* by regression using data from Fig. 10 we obtain

$$m = 1.30812 \times 10^8, \quad n = -2.54802.$$

The value of *b* is considered to be related to the reaction mechanisms. Observing that *b* in the high-temperature region changed little and regarding devolatilization in the high-temperature region to occur according to the same reaction mechanism, the average value of *b* (740–904 °C) is obtained, which is given by

$$b = \frac{b_1 + b_2 + \ldots + b_q}{q} \quad (q = 1, 2, 3, \ldots), \tag{6}$$

where *q* is the number of *b* measured in the case of the same reaction mechanism. In this research, *q* = 3. Using data from Table 2:

$$b = \frac{0.48 + 0.46 + 0.43}{3} = 0.457.$$

The process determining b in the model I is the same as in Eq. (6) and model I can be rearranged to

$$t_{vc} = 6.56 d^{0.457}. \tag{7}$$

Substituting Eq. (5) into Eq. (1) gives a new form of t_{vc}

$$t_{vc} = a d^{b} = m T^{n} d^{b}, \tag{8}$$

where m is temperature coefficient characteristic of volatiles' combustion, n is temperature characteristic exponent of volatiles' combustion, and b is reaction mechanism exponent characteristic of volatiles' combustion. In this research, Eq. (8) is called model II.

Substituting m and n from the above obtained into Eq. (8) gives

$$t_{vc} = 1.30812 \times 10^{8} T^{-2.54802} d^{0.457}. \tag{9}$$

Let us note that m, n, and b are the characteristic numbers under variation in temperature and other operating conditions are constants. The characteristic number for the above may change when the operating conditions change.

Comparison with experiments

The comparison between the model predictions and the experiments is shown in the plots for the experiments performed at 850 °C under operating condition F. The results are shown in Fig. 11 and Table 3.

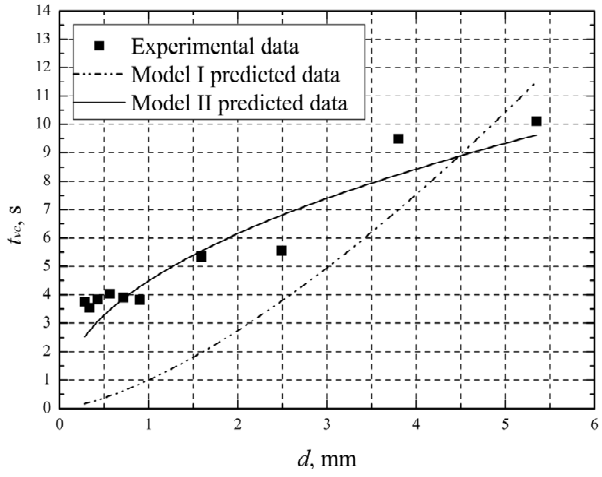

Fig. 11. Comparison of predicted and experimental data obtained at 850 °C under operating condition F.

Table 3. **The predicted and experimental data of volatile combustion time at 850 °**

Mean particle size, mm	Experimental data, s	Predicted data for model I, s	Predicted error for model I, %	Predicted data for model II, s	Predicted error for model II, %
5.35	10.11	11.51	13.88	9.62	4.83
3.80	9.50	6.99	26.38	8.24	13.25
2.49	5.56	3.78	32.05	6.80	22.27
1.59	5.35	1.97	63.26	5.55	3.65
0.90	3.83	0.86	77.61	4.28	11.95
0.72	3.91	0.62	84.15	3.86	1.25
0.57	4.04	0.44	89.09	3.47	14.23
0.43	3.83	0.29	92.37	3.05	20.36
0.34	3.55	0.21	94.15	2.73	22.92
0.28	3.76	0.16	95.84	2.53	32.75

From Table 3 we can see that the predicted error in the case of model I increases as particle size decreases. The error varies from 13.88% to 95.84%. The error of a in model I is great for the transient phenomenon like volatiles' combustion of oil shale. The minimum error of the model II between model predictions and experiments is 1.25%, the maximum error is 32.75%, the average error is 14.75%, and the average error for 0.57–5.35 mm particles is 10.2%. The error for particle sizes of 2.49 mm and 0.28–0.43 mm is more than 20% in the model I. It is likely that the components of oil shale may be changed after sieved by screens. Meanwhile, observation error may be introduced because of the short devolatilization time. In general, the values predicted by the new model (model II) have a smaller degree of error than values generated by model I. The new model can reflect the volatile combustion time of oil shale more accurately.

Analysis and prospects

From analysis above we can summarize the steps for obtaining volatile combustion time of oil shale as follows:

1. Obtaining data for volatile combustion time (t_{vc}) versus mean particle sizes (d) under $q'(q' \geq 3)$ sets of different temperature;
2. Assuming that t_{vc} satisfies Eq. (1) and regressing t_{vc} and d at some temperature T_i we obtain a_i and b_i (i = 1, 2, 3… q');
3. Assuming that a and T satisfy Eq. (5), regressing $q'(q' \geq 3)$ sets of a_i and T_i (i = 1, 2, 3… q') we obtain m and n;
4. Analyzing the value of b and using the average of q (q = 1, 2, 3…) sets of b for the same reaction mechanism (where the value of b changes a little) we get the final b in the model, namely as Eq. (6);
5. Substituting Eq. (5) into Eq. (1) gives the new expression for volatile combustion time as Eq. (8).

6. This model focuses on the effects of temperature but not other factors. Actually, the devolatilization of oil shale is a complex process, and other factors such as shale type, fragmentation, reactor type, mass and heat transfer, reaction atmosphere, pressure, and particle size distribution may have effects on devolatilization. We suggest that the new model should use a wider range of initial conditions in the future.

Conclusions

1. The proportion of volatiles' combustion near the bed decreases with increasing bed temperature, fluidization velocity and decreasing particle size. So, the furnace should have a sufficient height to ensure the heat be absorbed sufficiently to improve combustion efficiency.
2. The preheating time and burnout time decrease with increasing temperature particle size being the same and decrease with increasing particle size at the same temperature.
3. The combustion time of volatile matter of oil shale decreases slightly with increasing batch mass, fluidization velocity, and moisture content. In general, these three factors slightly affect devolatilization time.
4. The combustion time of volatile matter of oil shale is in accordance with the empirical model. A new modified model related to temperature, particle size, and reaction mechanisms under certain operating conditions was proposed. The presented model is found to be in agreement with experimental data. The model can facilitate predicting the combustion of volatiles in oil shale.
5. More reaction factors should be considered and much further research is needed to be carried out.

Acknowledgments

The authors are grateful for financial support from the National Natural Science Foundation of China (Grant 50876018) and the Key Project of Research Program of Jilin Province (20075015).

REFERENCES

1. *Wang, Q., Bai, J. R., Sun, B. Z., Sun, J.* Strategy of Huadian oil shale comprehensive utilization // Oil Shale. 2005. Vol. 22, No. 3. P. 305–316.
2. *Jaber, J. O., Probert, S. D.* Pyrolysis and gasification kinetics of Jordanian oil shales // Appl. Energ. 1999. Vol. 63, No. 4. P. 269–286.
3. *Khraisha, Y. H.* Batch combustion of oil shale particles in a fluidized bed reactor // Fuel Process. Technol. 2005. Vol. 86, No. 6. P. 691–706.
4. *Pillai, K. K.* The influence of coal type on devolatilization and combustion in fluidized beds. // J. Inst. Energ. 1981. Vol. 54, P. 142–150.

5. *Ross, D. P., Heidenreich, C. A., Zhang, D. K.* Devolatilisation times of coal particles in a fluidised–bed // Fuel. 2000. Vol. 79, No. 8. P. 873–883.
6. *Agarwal, P. K., Genetti, W. E., Lee, Y. Y.* Model for devolatilization of coal particles in fluidized beds // Fuel. 1984. Vol. 63, No. 8. P. 1157–1165.
7. *Bai, J. R., Dou, H. Q., Sun, B. Z., Wang, Q., Li, S. H., Sun, J.* Burn-out characteristics of oil shale blended with semi-coke // Journal of Power Engineering. 2007. Vol. 27, No. 5. P. 815–818 [in Chinese].
8. *Chern, J. S., Hayhurst, A. N.* Does a large coal particle in a hot fluidised bed lose its volatile content according to the shrinking core model? // Combust. Flame. 2004. Vol. 139, No. 3. P. 208–221.
9. *Saxena, S. C.* Devolatilization and combustion characteristics of coal particles // Prog. Energ. Combust. 1990. Vol. 16, No. 1. P. 55–94.
10. *Saastamoinen, J. J.* Simplified model for calculation of devolatilization in fluidized beds // Fuel. 2006. Vol. 85, No. 17–18. P. 2388–2395.
11. *Zheng, E. H., Wang, Q., Hao, Z. J.* The experimental study on ignition and combustion characteristics of Huadian oil shale-fired fluidized bed boiler // Clean Coal Technology. 2001. Vol. 7, No. 4. P. 41–45 [in Chinese].
12. *Zhang, H. T., Cen, K., Yan, J. H., Ni, M. J.* The fragmentation of coal particles during the coal combustion in a fluidized bed // Fuel. 2002. Vol. 81, No. 14. P. 1835–1840.
13. *Agarwal, P. K., Genetti, W. E., Lee, Y. Y.* Devolatilization of large coal particles in fluidized beds //Fuel. 1984. Vol. 63, No. 12. P. 1748–1752.
14. *Winter, F., Prah, M. E., Hofbauer, H.* Temperatures in a fuel particle burning in a fluidized bed: The effect of drying, devolatilization, and char combustion // Combust. Flame. 1997. Vol. 108, No. 3. P. 302–314.
15. *Sun, X. X., Chen, J. Y.* Physical and Chemical Basis of Pulverized Coal Combustion. – Wuhan: Huazhong University of Science and Technology Press, 1991 [in Chinese].
16. *Cen, K. F., Yao, Q., Luo, Z. Y., Li, X. T.* Advanced Combustion Theory. – Hangzhou: Zhejiang University Publishing House, 2002 [in Chinese].
17. *Paul, J., Peeler, K., Poynton, H. J.* Devolatilization of large coal particles under fluidized bed conditions // Fuel. 1992. Vol. 71, No. 4. P. 425–430.

Presented by Jialin Qian
Received November 16, 2009